Applied Catalysis A: General 486 (2014) 115–122

Contents lists available at ScienceDirect

Applied Catalysis A: General

journal homepage: www.elsevier.com/locate/apcata

Methanation of carbon dioxide on metal-promoted mesostructured silica nanoparticles

M.A.A. Aziz[a], A.A. Jalil[a,b], S. Triwahyono[c,*], S.M. Sidik[a]

[a] Institute of Hydrogen Economy, Universiti Teknologi Malaysia, 81310 UTM Johor Bahru, Johor, Malaysia
[b] Department of Chemical Engineering, Faculty of Chemical Engineering, Universiti Teknologi Malaysia, 81310 UTM Johor Bahru, Johor, Malaysia
[c] Department of Chemistry, Faculty of Science, Universiti Teknologi Malaysia, 81310 UTM Johor Bahru, Johor, Malaysia

ARTICLE INFO

Article history:
Received 22 June 2014
Received in revised form 5 August 2014
Accepted 19 August 2014
Available online 28 August 2014

Keywords:
CO_2 methanation
Mesostructured silica nanoparticles
Metal site
Basic sites
Oxygen vacancy site

ABSTRACT

Metal-promoted mesostructured silica nanoparticles (MSN) have been studied for CO_2 methanation under atmospheric pressure. In term of activities, high activity was observed on Rh/MSN, Ru/MSN, Ni/MSN, Ir/MSN, Fe/MSN and Cu/MSN at and above 623 K. However, on an areal basis, Ni/MSN was the most active catalyst, while Ir/MSN was the poorest catalyst. The catalysts have also been studied for elucidation of the role of each metal, MSN and metal/MSN in CO_2 methanation by *in situ* FTIR spectroscopy studies. Firstly, CO_2 and H_2 was adsorbed and dissociated on metal sites to form CO, O and H atoms, followed by migration onto the MSN surface. The dissociated CO then interacted with oxide surfaces of MSN to form bridged carbonyl and linear carbonyl, while the presence of H atom facilitated the formation of bidentate formate. These three species could be responsible for the formation of methane. However, the bidentate formate species could be the main route to formation of methane. MSN support has been found to play an important role in the mechanism. MSN support served the sites for carbonyl species which act as precursors to methane formation. These results provided new perspectives in the catalysis, particularly in the recycling of CO_2.

1. Introduction

The growing interest on greenhouse gas mitigation implies that CO_2 will be increasingly considered as a valuable feedstock for chemical industry instead of as a waste [1]. The valorization of carbon dioxide emissions could be one important part of the general strategy for reducing CO_2 emissions, and push chemical and energy companies towards a more sustainable use of the resources. There are several ways of adding value to CO_2, one of which is hydrogenation to form methane. Provided that hydrogen is generated from renewable energy sources such as water electrolysis [2], the methane produced by this reaction can be sent to chemical industry or can be utilized as an energy vector, which is an important advantage considering that the infrastructure for methane storage and transport is already present. CO_2 methanation has been investigated over a variety of supported metal catalysts, including Ni [3–11], Ru [12,13], Rh [14–17], Fe [18] and Cu [19]. Nickel catalysts were found to exhibit high activity for the reaction [4,5]. However, most of the studies concerning the methanation of CO_2 over Ni catalysts have been focused on the reaction performed at high temperatures (>473 K) [7,8]. In addition to Ni catalysts, CO_2 methanation has been studied by several authors using different noble metals such as Ru, Pd and Rh over a variety of supports. Among them, Rh has been shown to be one of the most promising metal catalyst that is active in low-temperature of reactions [14,16].

There is still no consensus about the mechanistic path of CO_2 methanation, even though it is a comparatively simple reaction. Thus, its reaction mechanism appears to be difficult to establish. In general, the proposed mechanism in the previous work fall into two main categories. The first mechanism involves the conversion of CO_2 to CO prior to methanation [20–22]. The other involves the direct hydrogenation of CO_2 to methane without forming CO as an intermediate [23,24]. The present work tends to fall into the first category. However, there are still different opinions on the nature of the intermediate and the methane formation process. For example, Betta and Shellef demonstrated the presence of formate in the hydrogenation of CO on a Ru/Al_2O_3 catalyst by IR spectroscopy. It was claimed that the formate ion was formed directly on the alumina support and its formation did not require metallic Ru [25]. Karelovic et al. studied CO_2 adsorption and dissociation on a Rh/γ-Al_2O_3 system in the presence of H_2 by operando-diffuse reflectance Fourier transform infrared spectroscopy (DRIFTS) experiments.

* Corresponding author. Tel.: +60 7 5536076; fax: +60 7 5536080.
E-mail addresses: sugeng@utm.my, sugengtw@gmail.com (S. Triwahyono).

http://dx.doi.org/10.1016/j.apcata.2014.08.022
0926-860X/

Their results showed that the linear Rh-CO species act as precursors of methane [14]. The mechanism of CO_2 methanation over Ni catalyst has been discussed by several authors [9,10,20,22]. One of the most cited mechanism proposes that the reverse water–gas-shift reaction, which generates CO from CO_2, is the first step. This reaction occurs on Ni surface and is followed by the methanation of CO. Falconer and Zagli studied the mechanism of CO_2 methanation over a Ni/SiO_2 catalyst, and reported that the carbon dioxide did not adsorb significantly on silica, leading them to conclude that this activated adsorption occurred on the nickel metal and not the support. Their conclusion was based on the capacity of CO_2, which did not adsorb significantly on SiO_2 [20]. Peebles et al. also suggested that CO_2 is quickly transformed into CO on the Ni surface [22]. However, the previously proposed mechanism leaves several questions unanswered regarding how the CO_2 is adsorbed and transformed into methane:

(i) CO_2 methanation over unsupported Ni exhibited low yield of methane. Therefore, it is difficult to conclude that the CO that adsorbed on the Ni and/or metal surface was a precursor to methane.
(ii) The technique used to elucidate the mechanism of CO_2 methanation was performed on a combination of metal and support, and it was difficult to determine the real function of the metal and the support. Therefore, each metal, support and metal/support combination should be tested in order to know the role of their presence.

Therefore, in this work, a series of metal-based catalyst supported on mesostructured silica nanoparticles (M/MSNs; M = Rh, Ru, Ni, Fe, Ir, Cu, Zn, V, Cr, Mn, Al and Zr) were prepared, and were applied for methane production from carbon dioxide and hydrogen gas in the temperature range of 373–723 K under atmospheric pressure. The effect of metal on the MSN was characterized by X-ray diffraction (XRD), nitrogen physisorption and infrared spectroscopy. To elucidate the mechanistic path of CO_2 methanation, *in situ* FTIR spectroscopy was used to observe the surface species during the reaction.

2. Experimental

2.1. Catalyst preparation

MSN was prepared by the sol–gel method according to the report by Karim et al. [26]. The surfactant cetyltrimethylammonium bromide (CTAB; Merck), ethylene glycol (EG; Merck) and NH_4OH solution (QRec) were dissolved in water with the following molar composition of $CTAB:EG:NH_4OH:H_2O = 0.0032:0.2:0.2:0.1$. After vigorous stirring for about 30 min at 353 K, 1.2 mmol of tetraethyl orthosilicate (Merck) and 1 mmol of 3-aminopropyl triethoxysilane (Merck) were added to the clear mixture to give a white suspension solution. This solution was then stirred for another 2 h, and the samples were collected by centrifugation at 20,000 rpm. The as-synthesized MSN were dried at 333 K and calcined at 823 K for 3 h in air to remove the surfactant. For unsupported Ni catalyst, it was prepared by calcination of $Ni(NO_3)_2{\cdot}6H_2O$ at 823 K for 3 h. For metal based MSN catalysts, they were prepared by impregnation of MSN powder with an aqueous solution of the corresponding metal salt precursor ($RhCl_3$, $RuCl_3$, $Ni(NO_3)_2$, $IrCl_3$, $Fe(NO_3)_3$, $Cu(CO_2CH_3)_2$, $Zn(NO_3)_2$, $V(C_5H_7O_2)_3$, $Cr(NO_3)_3$, $MnCl_2$, $Al(NO_3)_3$ and $ZrOCl_2$) (Merck, 99%). The resulting slurry was heated slowly at 353 K under continuous stirring and maintained at that temperature until nearly all the water being evaporated. The solid residue was dried in an oven at 383 K overnight before calcination at 823 K for 3 h in air. The metal loading of the catalysts was 5 wt%. All metal based MSN samples were denoted as Rh/MSN, Ru/MSN, Ni/MSN, Ir/MSN, Fe/MSN, Cu/MSN, Zn/MSN, V/MSN, Cr/MSN, Mn/MSN, Al/MSN and Zr/MSN.

2.2. Characterization

The crystalline structure of the catalyst was determined by X-ray diffraction (XRD) recorded on a powder diffractometer (Bruker Advance D8, 40 kV, 40 mA) using a Cu Kα radiation source in the range of $2\theta = 1.5–90^\circ$. The BET analysis of the catalyst was determined by N_2 adsorption–desorption isotherms using a Quantachrome Autosorb-1 instrument. The catalyst was outgassed at 573 K for 3 h before being subjected to N_2 adsorption. Pore size distributions and pore volumes were determined from the sorption isotherms using a non-localized density functional theory (NLDFT) method. In the FTIR measurements, pyrrole has been used as a probe molecule for the characterization of basic sites [3]. The methanation was also recorded by *in situ* FTIR spectroscopy to study the surface species formed during the reaction. All the measurements were performed on an Agilent Cary 640 FTIR spectrometer equipped with a high-temperature stainless steel cell with CaF_2 windows. Prior to the measurements, 30 mg of sample in the form of a self-supported wafer was reduced in H_2 stream (100 ml/min) at 773 K for 4 h and cooling to 303 K under He atmosphere. For pyrrole adsorption, the reduced catalyst was exposed to 2 Torr of pyrrole at 303 K for 30 min, followed by outgassing at 423 K for 30 min. All spectra were recorded at room temperature with a spectral resolution of 5 cm^{-1} with five scans. Furthermore, the formation of surface species during the methanation was recorded by introducing of a mixture of CO_2 (4 Torr) and H_2 (16 Torr) to the catalyst at room temperature, followed by heating to 523 K. The spectra were recorded after equilibrium conditions have been reached. For CO_2 and H_2 adsorption studies, the sample was pretreated using the same procedure as above. The adsorption of CO_2 was done by exposing 4 Torr of CO_2 on sample at room temperature and subsequent heating to 523 K. While, the adsorption of H_2 was done by exposing 16 Torr H_2 at room temperature followed by heating in hydrogen from 303 to 573 K. For adsorption of CO_2, H_2 or the mixture of CO_2 and H_2 in the bare Ni catalyst, the Ni catalyst was mixed with KBr (Ni:KBr = 1:100) to increase the transparency of the sample.

2.3. Catalytic activity measurements

CO_2 methanation was conducted in a microcatalytic quartz reactor with an interior diameter of 8 mm at atmospheric pressure at temperature range of 373–723 K. The thermocouple was directly inserted into the catalyst bed to measure the actual pretreatment and reaction temperatures. The catalyst was sieved and selected in the 20–40 μm fraction. Initially, 200 mg of catalyst was treated in an oxygen stream (F_{Oxygen} = 100 ml/min) for 1 h followed by a hydrogen stream ($F_{Hydrogen}$ = 100 ml/min) for 4 h at 773 K and cooled down to the desired reaction temperature in a hydrogen stream. After the temperature became stable, a mixture of H_2 and CO_2 was fed into the reactor at gas hourly space velocity (GHSV) of 50,000 ml g^{-1} h^{-1} and H_2/CO_2 mass ratio of 4/1. All gases were controlled with calibrated mass flow controllers (SEC-400 MK2, Stec Ltd., Japan). The CH_4 formation rate was measured in the temperature range of 373–723 K. The activity was monitored with decreasing temperature and back to verify stable catalyst conditions during these measurements. The composition of the outlet gases was analyzed with an on-line 6090N Agilent gas chromatograph equipped with a GS-Carbon PLOT column and a TCD detector. The lines from the outlet of the reactor to the GC were heated at 383 K to avoid condensation of the products. The moisture trap was installed at the outlet gas line of the reactor to prevent moisture

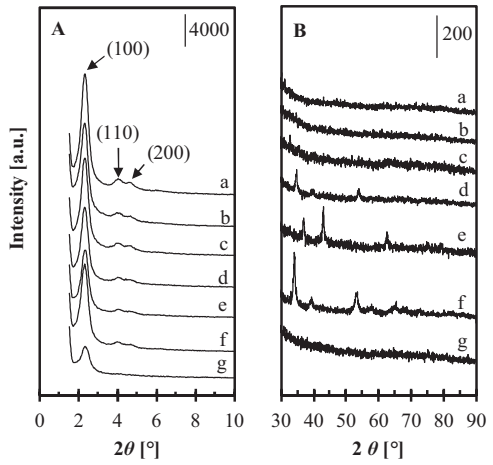

Fig. 1. (A) Low-angle and (B) wide-angle XRD patterns of (a) MSN, (b) Rh/MSN, (c) Fe/MSN, (d) Ru/MSN, (e) Ni/MSN, (f) Ir/MSN and (g) Cu/MSN.

from entering the GC. To determine the activity and selectivity, the products were collected after 1 h of steady-state operation at each temperature. The conversion of carbon dioxide, selectivity of products, rate of methane formation and areal rate were calculated by the following equations:

$$X_{CO_2}(\%) = \frac{F_{CO_2,in} - F_{CO_2,out}}{F_{CO_2,in}} \times 100\% \quad (1)$$

$$S_x(\%) = \frac{F_{X,out}}{F_{CO_2,in} - F_{CO_2,out}} \times 100\% \quad (2)$$

$$\text{rate}(\text{mol}_{CH_4}\ \text{mol}_{Metal}^{-1}\ \text{s}^{-1}) = \frac{F_{X,out}}{\text{mole of } M_{Total}} \quad (3)$$

$$\text{Areal rate}(\text{mmole}_{CH4} \times \text{m}^{-2}\ \text{s}^{-1}) = \frac{F_{X,out}}{S_{BET} \times W_{cat}} \quad (4)$$

where X_{CO_2} is the conversion of carbon dioxide (%), S_x is the selectivity of x product (%) in which x is a CH_4 or CO, F is a molar flow rate of CO_2 or product in mole per second, M_{Total} is the total amount of metal in mole, S_{BET} is the surface area of the catalysts and W_{cat} is the weight of catalysts.

3. Results and discussion

3.1. Characterization of materials

Fig. 1A shows the small-angle XRD patterns of MSN and metal-based MSN catalysts. The patterns exhibited three peaks, indexed as (1 0 0), (1 1 0) and (2 0 0), which are reflections of the typical two-dimensional hexagonally ordered mesostructure (*p6mm*), demonstrating the high quality of mesopore packing [27]. The ordered MSN support structure was disturbed slightly by the presence of metals. No shift of peaks was observed, but the intensities decreased with the introduction of metal. The intensity was in the order Rh/MSN > Fe/MSN > Ru/MSN > Ni/MSN > Ir/MSN > Cu/MSN, indicating a structural degradation of MSNs. The presence of metal crystallites on the catalysts were characterized using wide-angle XRD (30–90°), as shown in Fig. 1B. No diffraction peaks ascribed to Rh, Fe and Cu species on MSNs were detected, indicating that either the metal particles were smaller in diameter than the detection limit (*ca.* 4 nm) of the diffractometer, or the large metal particles (>4 nm) were too scarce to produce detectable diffraction signals. XRD pattern of Ru/MSN showed the diffraction peaks of ruthenium oxide species (RuO_2) at 28°, 35° and 54° with small diffraction of ruthenium metal species (Ru) at 40° [28]. For Ni/MSN, the diffraction peaks at 37.3°, 43.2°, 62.9°, 75.3° and 79.4° were attributed to a face-centered cubic crystalline NiO [5]. The XRD pattern of Ir/MSN showed the diffraction peaks at 27.5°, 34.5°, 38°, 52.9°, 56° and 63°, attributed to the Ir species in an oxide form (IrO_2) [29].

The porosity of catalysts was measured by the N_2 physisorption method. The location of the inflection point is related to the pores at the mesoscale, and the sharpness of these curves reveals the uniformity of the mesopore size distribution [30]. Fig. 2A and B shows the adsorption–desorption isotherms of all catalysts. All isotherm curves exhibited two capillary condensation steps. The first step in a relative pressure range of P/P_o = 0.3–0.4 was attributed to the nitrogen condensation that took place at the internal mesopores. There was no hysteresis loop in this capillary condensation. The second step above P/P_o = 0.95 in the adsorption branch was due to the presence of interparticle voids [31]. A small hysteresis loop at this relative pressures was ascribed to the condensation of nitrogen within the interstitial voids or interparticle textural porosity created by MSN particles, which indirectly reflects the size of particles, i.e. a higher partial pressure was associated with a smaller particle size. However, almost no change in relative pressure at P/P_o = 0.95 indicates that the particle size of the MSNs was maintained after introduction of the metal. The inflection points were similar but the sharpness of the steeps decreased after introduction of the metal. For instance, almost no steeps were observed on Ru/MSN and Cu/MSN in the first condensation step indicating the low uniformity of micropores of the catalysts. In addition, low uniformity of mesopores was observed only on Cu/MSN, since the steep in the second condensation markedly decreased after introduction of Cu.

Textural parameters of MSNs and metal-based MSN catalysts are summarized in Table 1. All samples possessed high surface area, typically larger than 800 $m^2\ g^{-1}$, except for Cu/MSN, which had a surface area of 501 $m^2\ g^{-1}$. The impregnation of a small amount of metal (Rh, Fe, Ru, Ni, Ir and Cu) produced little effect on the pore diameter. It is obvious that the nitrogen adsorption decreased with increased of pore size. The introduction of metal on MSNs also affected the micropore and mesopore distribution of the catalysts (Fig. 2C and D). All catalysts showed a bimodal pore structure consisting of framework mesopores of 20–30 Å and textural mesopores in the range 100–1000 Å. However, Cu/MSN showed no pore distribution in the range 20–30 Å, but had a pore distribution in the range 35–45 Å.

FTIR spectroscopy in the skeletal region at 1300–700 cm^{-1} was used to follow the variation of the structure of metal-based MSNs. Typical absorbance bands due to siliceous material Si—O—Si were observed for bare MSN and metal-based MSNs (Fig. 3A). The bands at approximately 1200 and 1080 cm^{-1} were ascribed to the longitudinal and transverse optical modes of the asymmetric Si—O stretching vibration. Two weaker bands at approximately 960 and 805 cm^{-1} were attributed to Si—OH and the symmetric Si—O stretching vibration, respectively. The band at 960 cm^{-1} is attributed to the presence of transition metal atoms near the silica framework as the stretching Si—O vibration mode perturbed by the neighboring metal ions. Therefore, a shift of the absorbance band at 960 cm^{-1} indicated a structural change for the surface Si—OH group caused by the presence of metal species in the MSN, and/or due to evolution of a new band of Si—O—M. The absorbance band of MSN at 960 cm^{-1} shifted to 958, 973, 970 and 975 cm^{-1} for Rh/MSN, Fe/MSN, Ru/MSN and Ir/MSN, respectively. However, no shift was observed for Ni/MSN and Cu/MSN indicating that the Ni and Cu did not interact with the MSN framework. Reduced MSNs and metal-based MSNs possessed an intense band at 3740 cm^{-1} with a shoulder at 3710 cm^{-1} and a broad halo centered around 3650 cm^{-1} (Fig. 3B). The bands at 3740 and 3710 cm^{-1} are unambiguously assigned to

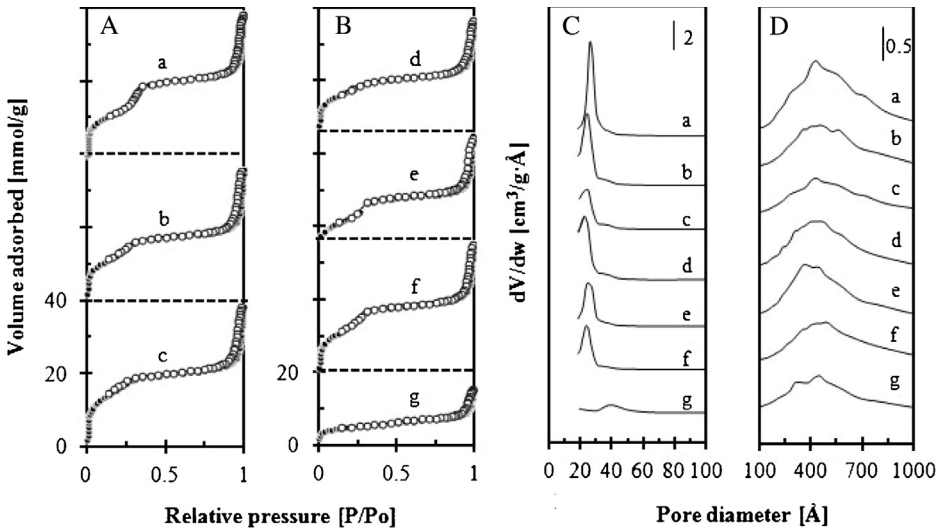

Fig. 2. N_2 adsorption–desorption isotherms (A, B) and NLDFT pore size distribution (C, D) of (a) MSN, (b) Rh/MSN, (c) Fe/MSN, (d) Ru/MSN, (e) Ni/MSN, (f) Ir/MSN and (g) Cu/MSN.

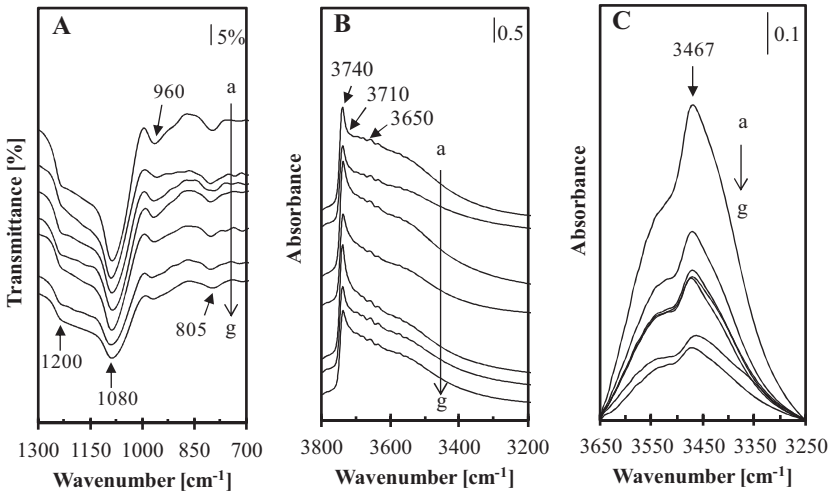

Fig. 3. FTIR spectra of (A) fresh and (B) reduced catalysts: (a) MSN, (b) Rh/MSN, (c) Fe/MSN, (d) Ru/MSN, (e) Ni/MSN, (f) Ir/MSN and (g) Cu/MSN. (C) Normalized IR spectra of pyrrole adsorbed on reduced catalysts of (a) MSN, (b) Ru/MSN, (c) Fe/MSN, (d) Rh/MSN, (e) Ni/MSN, (f) Cu/MSN and (g) Ir/MSN.

terminal (isolated) and internal silanol groups, respectively. The broad absorbance is indicative of the presence of H-bonded hydroxyls. The result showed the decrease in intensity of a silanol band at 3740 cm^{-1} upon the incorporation of metal, suggesting a perturbation of the silica framework upon interaction with metal [32].

The presence of basic sites on metal based MSN was evidenced by pyrrole adsorption–desorption FTIR spectroscopy. The H-donor

Table 1
Physicochemical properties and catalytic performance. The reaction was done at 623 K with GHSV of 50,000 ml g^{-1} h^{-1} and H_2/CO_2 ratio of 4/1.

Catalyst	S_{BET} (m^2 g^{-1})	V_{pore} (cm^3 g^{-1})	d_{pore} (Å)	Rate × 10^{-2} (mol_{CH4} mol_{Metal}^{-1} s^{-1})	Conversion, X_{CO_2} (%)	Selectivity (%)[a]		Areal rate × 10^{-3} ($mmol_{CH4}$ m^{-2} s^{-1})
						CH_4	CO	
Ni	3	0.016	194	–	0.5(1.5)[c]	100[b] (0)[c]	0[b] (100)[c]	–
MSN	1051	0.758	28	–	0.3	0[b]	100[b]	–
Rh/MSN	933	0.910	36	29.71	99.5	100	0	0.966
Ru/MSN	1004	0.934	37	28.42	95.7	100	0	0.885
Ni/MSN	879	0.798	34	25.39	85.4	99.9	0.1	1.554
Ir/MSN	976	0.723	33	2.81	9.5	83	17	0.047
Fe/MSN	858	0.805	35	0.97	4	92	8	0.064
Cu/MSN	501	0.642	32	0.57	3.3	79	21	0.057

S_{BET}: BET surface area; V_{pore}: total pore volume; d_{pore}: average pore diameter.
[a] Selectivity at conversion = 20%.
[b] Selectivity at conversion = 0.3%.
[c] The result in the parenthesis shows the reaction in the presence of CO_2 only.

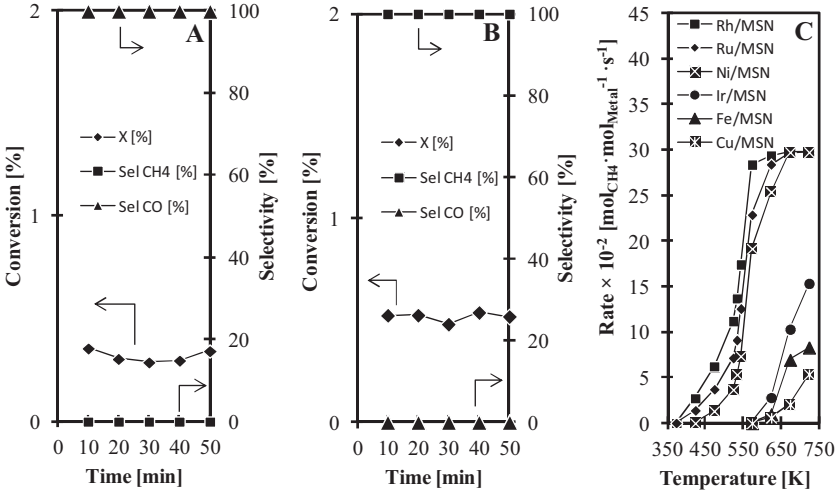

Fig. 4. Catalytic activity of (A) MSN and (B) Ni at 623 K. (C) Catalytic activity of various metal based MSN at steady state condition as a function of reaction temperature.

pyrrole properties allow $C_4H_4NH\cdots O$ bridges to form with basic oxygen in the framework [33]. It was shown by pyrrole adsorption and desorption experiments that ≡Si—O⁻ species could play a role as an oxidizing center. Pyrrole adsorbed on MSNs and metal-based MSNs verified the formation of hydrogen-bonded species of pyrrole as observed in the IR spectra around 3467 cm^{-1} (Fig. 3C). The introduction of metal, however, partially blocked the basic sites of the catalyst and thus reduced the chemisorptions of pyrrole on the catalyst. Each metal has different behavior on the blocking effect of metal on the pyrrole adsorption. For example, Rh/MSN has lower tendency to produce the blocking effect due to its high metal dispersion. In contrast, Cu/MSN has a higher blocking effect due to its low metal dispersion. The basic sites have a close relationship with the structure defects or oxygen vacancy, which was explained in previous studies [3,34–37]. For instance, the calcination of mixed Al_2O_3–MgO produces high surface area and number of defect sites (the number of oxygen atoms associated with Mg exhibiting a low coordination number), and this leads to higher basicity [34]. Therefore, it may be stated that the basic or oxygen vacancy sites can be dedicated as active sites for the CO_2 adsorption. This indicated that Ru- and Cu-based MSNs possess highest and lowest concentration of oxygen vacancy sites, respectively.

3.2. Catalytic performance

The results of the catalytic reactions are summarized in Fig. 4 and Table 1. For MSN (Fig. 4A), the conversion of CO_2 at 623 K was only around 0.3% with 100% selectivity to CO. Low conversion of MSN was due to the absence of metal sites, which is crucial for H_2 and CO_2 dissociation. For Ni, two types of reactions occurred (Fig. 4B and Table 1). In the absence of H_2, the conversion of CO_2 reached around 1.5% with 100% selectivity for CO. No methane products were observed due to the absence of H_2. In the presence of H_2, the conversion of CO_2 decreased to around 0.5% with 100% selectivity for methane. The 67% decrease of conversion was probably due to the competitive adsorption–dissociation of CO_2 and H_2 on the surface of metallic Ni [38] and the absence of a MSN support, which facilitated the formation of surface carbonyl species. In addition, the low conversion may also be due to the absence of metal–support interaction, which served to increase the metal dispersion [4]. Riani et al. also reported that Ni was inactive in CO_2 methanation in which the results gave no conversion of CO_2 at 573 K [39]. These results explained the inability of unsupported metal catalysts for CO_2 methanation. Therefore, in general, the unsupported metal catalysts (Ni, Rh, Fe, Ru, Ir and Cu) were presumed to be inactive for CO_2 methanation.

For metal-based MSNs (Fig. 4C), the rate of methane formation ($mol_{CH4}\,mol_{metal}^{-1}\,s^{-1}$) is plotted as a function of reaction temperature in the range 373–723 K. *S*-curves results were observed for all catalysts indicating that the rate production of methane was not influenced by intraparticles diffusion of the catalysts under the present reaction conditions. Furthermore, the order of the activity for CO_2 methanation at 623 K was Rh/MSN > Ru/MSN > Ni/MSN > Ir/MSN > Fe/MSN > Cu/MSN. For Rh/MSN and Ru/MSN, the reaction started at 423 K and the conversion of CO_2 reached 100% at 673 K and the activity continued till 723 K.

For Ni/MSN, the reaction began at 473 K and the conversion reached 100% at 673 K. The CO_2 methanation increased rapidly at 523 K over these three catalysts. Indeed, the Rh/MSN, Ru/MSN and Ni/MSN could catalyze CO_2 methanation at and below 473 K. In particular, the catalytic activity of Rh/MSN was the highest, compared to other catalysts, at and below 573 K, while Ir/MSN, Fe/MSN and Cu/MSN were practically inactive below 573 K. In fact, high reaction temperature (>723 K) is required in order to achieve CO_2 conversions above 10% over these latter catalysts. It is also a common practice to compare catalyst activities based on catalyst surface area rather than catalyst mass. The final column in Table 1 provides the catalytic rates based on area (areal rates) for all metal based MSN catalysts at 623 K. The activity order was Ni/MSN > Rh/MSN > Ru/MSN > Fe/MSN > Cu/MSN > Ir/MSN. By contrast, using this measure of activity, Ni/MSN was the most active catalyst, while Ir/MSN was the poorest catalyst. These results suggest that Rh, Ru, or Ni metal on MSN are effective catalysts for methanation of CO_2 in the temperature range 423–573 K, while Ir, Fe or Cu metal on MSN are active in the temperature range 623–723 K. In addition, no activity (methane production) was observed on Zn/MSN, V/MSN, Cr/MSN, Mn/MSN, Al/MSN and Zr/MSN in the temperature range studied. Therefore, the characterization data for these metal-based MSN catalysts are not shown or discussed in the present study.

3.3. Mechanistic investigation of CO_2 methanation

In the following sections, FTIR spectra were recorded on Ni, MSN, Ni/MSN, Rh/MSN and Fe/MSN catalysts under a set of defined adsorption conditions (Fig. 5). For Ni (inset in Fig. 5A), there was a strong band at around 450 cm^{-1}, which corresponds to the bending vibration of Ni—O bond [40]. The adsorption of CO_2, H_2 and

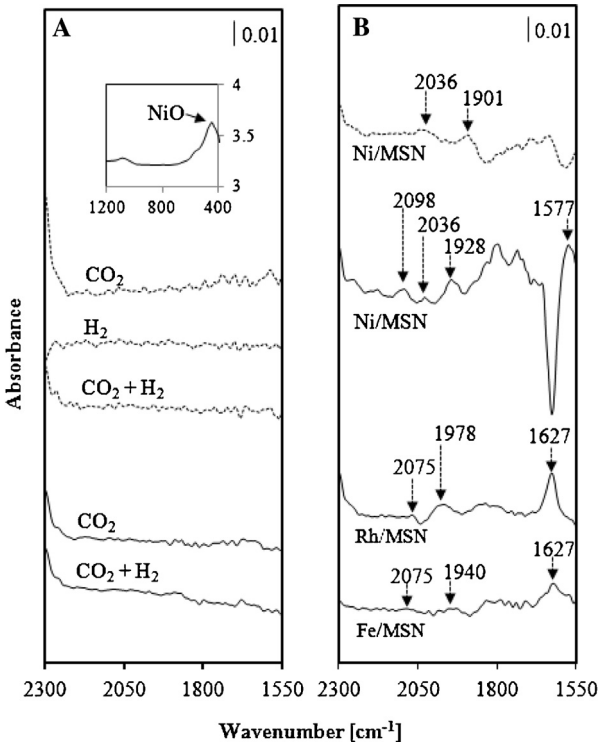

Fig. 5. (A) Evaluation of the FTIR spectra of adsorbed gases (CO_2, H_2 and $CO_2 + H_2$) on Ni (dotted lines) and MSN (true lines). Inset shows the FTIR spectra of Ni in range of 1200–400 cm^{-1}. (B) Evaluation of the FTIR spectra of adsorbed CO_2 (dotted lines) on Ni/MSN and $CO_2 + H_2$ (true lines) on Ni/MSN, Rh/MSN and Fe/MSN. All spectra of adsorbed gases were monitored at 523 K.

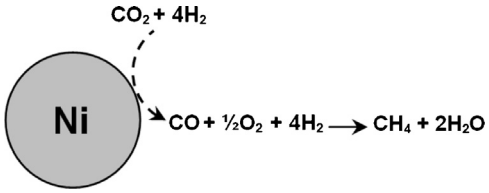

Scheme 1. Plausible mechanism of CO_2 methanation on Ni.

$CO_2 + H_2$ on Ni showed no significant bands. These results indicate that the methanation reaction on Ni probably takes place in the gas phase rather than on the catalyst surface, in agreement with the report by Medsford [41]. Therefore, a plausible mechanism of methanation on Ni is shown in Scheme 1.

The assumption of this phenomenon was also based on the inability of Ni to perform high methanation activity. In the case of Ni, as mentioned earlier, in the absence of H_2, the reaction performed on CO_2 resulted in CO product only. In contrast, when CO_2 and H_2 were applied during the reaction, only a small amount of methane was observed indicating that all CO was hydrogenated to methane. However, the percentage conversion of CO_2 on Ni was very low (0.3%) indicating that the CO_2 methanation was probably not taking place on the Ni surface. Similarly, the generation of adsorbed species was not observed on MSN (Fig. 5A). The absence of adsorbed species on MSN was due to the absence of Ni sites to dissociate CO_2 and/or H_2. Under CO_2 adsorption on Ni/MSN (Fig. 5B), two types of adsorbed species were observed at 2036 and 1901 cm^{-1}, which are attributed to linear and bridged carbonyl on the surface of MSN, respectively. From these result, it is presumed that the role of Ni was to dissociate the CO_2 into CO and O adsorbed species. The dissociated CO tends to migrate through the MSN surface (spillover) and then interacted with oxide surface of MSN to

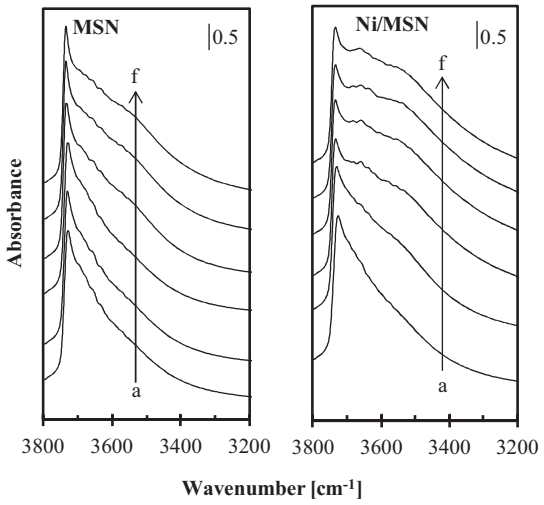

Fig. 6. The changes in the IR spectra when MSN and Ni/MSN were heated in 16 Torr of hydrogen at (b) 303 K, (c) 323 K, (d) 423 K, (e) 523 and (f) 573 K. (a) Before exposure to hydrogen. All samples were pretreated with hydrogen at 773 K for 4 h and cooling to 303 K under He atmosphere.

form carbonyl while another O fills the oxygen vacancy near the Ni sites.

The ability of Ni to dissociate H_2 was evidenced by *in situ* FTIR spectroscopy of H_2 adsorption on Ni/MSN. From the results (Fig. 6), the surface concentration of the hydroxyl groups increased with increasing temperature from 323 to 573 K in the presence of hydrogen. A larger increase was observed on Ni/MSN compared to MSN indicating that the supply of H atoms was higher in Ni/MSN compared to MSN. The ability of Ni, Rh and Fe metal to dissociate molecular H_2 was also previously discussed by several reports [42–44]. The MSN surface or oxygen vacancy site probably has a low ability to adsorb and dissociate molecular hydrogen to hydrogen atoms compared to Ni/MSN. A similar result was observed on a TiO_2 surface in which Menetrey et al. reported that the presence of an oxygen vacancy did not affect the adsorption–dissociation of hydrogen molecule [45]. The interaction of molecular hydrogen is lower on the oxygen vacancy containing TiO_2 than that on the perfect structure of TiO_2. Therefore, from the results, it can be suggested that the role of Ni was to dissociate H_2 and CO_2, followed by spillover of CO, O and H atoms onto the MSN surface and formation of methane and water. The detail mechanistic will be explained in further discussion.

In situ FTIR spectroscopy of $CO_2 + H_2$ at 523 K on metal based MSN is also presented in Fig. 5B. For Ni/MSN, Rh/MSN and Fe/MSN, the bands at 2098, 2075, 2036 cm^{-1} were assigned to linear carbonyl, while the bands at 1978, 1940 and 1928 cm^{-1} were assigned to bridged carbonyl in which both of the species were adsorbed onto surface oxygen. The last two bands at 1627 and 1577 cm^{-1} were assigned to adsorbed water and bidentate formate, respectively [46,47]. The negative band at 1627 cm^{-1} for Ni/MSN was attributed to water which have some degree of water termination. The CH_x and CO gases vibration bands, which known to appear at 2800–3000 cm^{-1} and 2100–2200 cm^{-1} regions, were not detected for any catalyst in this experiment. Based on these results, a plausible mechanism for CO_2 methanation on metal-based MSNs is shown in Scheme 2.

Firstly, CO_2 and H_2 was adsorbed onto metal sites, followed by dissociation to form CO, O and H atoms, and migration onto the MSN surface. The CO then interacted with oxide surfaces of the MSN to form bridged carbonyl and linear carbonyl. Bidentate formate was also formed through the interaction with atomic hydrogen. Meanwhile, the O atom spilt over onto the surface of

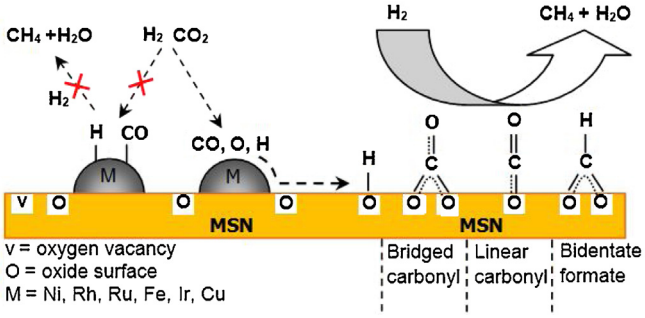

Scheme 2. Plausible mechanism of CO_2 methanation on M/MSN.

the MSN and was stabilized in the oxygen vacancy site near the metal site. The adsorbed oxygen then reacted with atomic hydrogen to form hydroxyl on the MSN surface in which a further reaction with another atomic hydrogen formed a water molecule. Finally, the adsorbed carbon species was further hydrogenated to methane and another water molecule. In this study, all three species (linear carbonyl, bridged carbonyl and bidentate formate) could be an intermediate for CO_2 methanation as reported by previous studies [9–11,14,17,25]. However, the bidentate formate species could be the main intermediate for CO_2 methanation as agreement by the previous studies [9–11]. Fujita et al. has reported that the hydrogenation has occurred on bridged carbonyl and formate species located on the support. Pan et al. has reported that the formate species were found to be the main intermediate species during the CO_2 methanation. Similarly, Aldana et al. also found that formate species were formed on the surface of catalysts and hydrogenated to form methane.

The results provide new evidence that helps in the understanding of the nature of the intermediate in the methane formation process, and a new pathway in the mechanism of CO_2 methanation has been presented in this study. The main finding is related to the ability of Ni to dissociates H_2 and CO_2 followed by migration onto the MSN surface. Such behavior apparently conflicts with prevalent opinion relating strong binding of CO with metal sites (M–CO) in which the M–CO species undergo methane formation [14–16]. Jacquemin et al. looked into the reaction mechanism of CO_2 methanation on Rh/γ-Al_2O_3 and found the dissociation of CO_2 into CO and oxygen on the surface of the catalyst, as evidenced by *in situ* DRIFT experiments [16]. Karelovic et al. studied the CO_2 adsorption and dissociation on a Rh/γ-Al_2O_3 system in the presence of H_2 by operando-DRIFTS experiments. Their result showed the formation of linear Rh-CO species that act as a precursors of methane [14]. In the case of Ni catalysts, Aldana et al. studied the mechanism of CO_2 methanation over Ni–Ceria/zirconia. They reported that the role of Ni is to dissociate H_2 while ceria–zirconia support was responsible to adsorb the CO_2 to form carbonates which would be hydrogenated into formates and further into methoxy species [9]. Pan et al. proposed that CO_2 was adsorbed onto hydroxyl and surface oxygen of ceria–zirconia to form bidentate and monodentate formate in the presence of hydrogen, respectively [10]. However, they did not discuss the detailed route of CO_2 adsorption onto the catalyst surface, although they did mention that CO_2 was activated on the surface oxygen of the ceria–zirconia support. Furthermore, under the experimental conditions used in this present work, the presence of metal carbonyls were not observed on metal (Ni, Rh and Fe). On the other hand, it may be suggested that the route to the methane formation was not formed via metal carbonyl. In summary, metal sites were identified and found to be responsible for dissociating CO_2 to form CO and O, followed by migration onto the catalyst's surface. While, MSN support was responsible to serve the sites for carbonyl species which act as precursor to methane formation.

4. Conclusions

Mesostructured silica nanoparticles (MSN) and a series of metal catalysts (Rh, Ru, Ni, Fe, Ir, Cu, Zn, V, Cr, Mn, Al and Zr) loaded on MSNs were prepared by a sol–gel and impregnation method for methanation of CO_2. The basic site of the catalysts were characterized on the basis of pyrrole adsorption–desorption study. The concentration of basic site altered with the type of metals in which Ru/MSN and Cu/MSN possessed the highest and lowest concentrations of basic sites, respectively. The results indicated that surface centers containing metallic and associated basic and/or oxygen vacancy sites are responsible for the active sites for this process. At 623 K, the catalytic activity changed in the order of Rh/MSN > Ru/MSN > Ni/MSN > Ir/MSN > Fe/MSN > Cu/MSN. Low conversion of CO_2 was observed on MSN, Ni, Zn/MSN, V/MSN, Cr/MSN, Mn/MSN, Al/MSN and Zr/MSN. In term of areal basis, Ni/MSN exhibited the most active catalyst while Ir/MSN is the poorest catalyst. Based on the FTIR studies, the detailed mechanism has been proposed for the methanation of CO_2 over metal-based MSNs. Firstly, CO_2 and H_2 is adsorbed and dissociated on metal sites to form CO, O and H atoms, followed by migration onto the MSN surface. The CO then interacts with oxide surfaces of the MSNs to form bridged carbonyl and linear carbonyl, while the presence of H atom facilitates the formation of bidentate formate. These three species could be responsible for the formation of methane. However, the bidentate formate species could be the main route to formation of methane. MSN support has been found to play an important role in the mechanism. MSN support served the sites for carbonyl species which act as precursor to methane formation. This proposed mechanism creates a new perspective and better understanding of the mechanisms of CO_2 methanation.

Acknowledgments

This work was supported by Ministry of Science, Technology and Innovation, Malaysia through EScienceFund Research Grant no. 03-01-06-SF0987, MyPhd Scholarship (Muhammad Arif Ab Aziz) from Ministry of Higher Education, Malaysia.

References

[1] M. Wang, Z. Wang, X. Gong, Z. Guo, Renew. Sustain. Energy Rev. 29 (2014) 573.
[2] G. Centi, S. Perathoner, Catal. Today 148 (2009) 191.
[3] M.A.A. Aziz, A.A. Jalil, S. Triwahyono, R.R. Mukti, Y.H. Taufiq-Yap, M.R. Sazegar, Appl. Catal. B 147 (2014) 359.
[4] Y.-H. Huang, J.-J. Wang, Z.-M. Liu, G.-D. Lin, H.-B. Zhang, Appl. Catal. A 466 (2013) 300.
[5] G. Zhang, T. Sun, J. Peng, S. Wang, S. Wang, Appl. Catal. A 462–463 (2013) 75.
[6] G. Du, S. Lim, Y. Yang, C. Wang, L. Pfefferle, G.L. Haller, J. Catal. 249 (2007) 370.
[7] B. Lu, K. Kawamoto, Fuel 103 (2013) 699.
[8] E. Jwa, S.B. Lee, H.W. Lee, Y.S. Mok, Fuel Process. Technol. 108 (2013) 89.
[9] P.A.U. Aldana, F. Ocampo, K. Kobl, B. Louis, F. Thibault-Starzyk, M. Daturi, P. Bazin, S. Thomas, A.C. Roger, Catal. Today 215 (2013) 201.
[10] Q. Pan, J. Peng, S. Wang, S. Wang, Catal. Sci. Technol. 4 (2014) 502.
[11] S. Fujita, M. Nakamura, T. Doi, N. Takezawa, Appl. Catal. A 104 (1993) 87.
[12] A.-X. Yin, W.-C. Liu, J. Ke, W. Zhu, J. Gu, Y.-W. Zhang, C.-H. Yan, J. Am. Chem. Soc. 134 (2012) 20479.
[13] J.H. Kwak, L. Kovarik, J. Szanyi, ACS Catal. 3 (2013) 2449.
[14] A. Karelovic, P. Ruiz, ACS Catal. 3 (2013) 2799.
[15] A. Beuls, C. Swalus, M. Jacquemin, G. Heyen, A. Karelovic, P. Ruiz, Appl. Catal., B 113–114 (2012) 2.
[16] M. Jacquemin, A. Beuls, P. Ruiz, Catal. Today 157 (2010) 462.
[17] J.J. Benítez, R. Alvero, M.J. Capitán, I. Carrizosa, J.A. Odriozola, Appl. Catal. 71 (1991) 219.
[18] H.M.T. Galvis, J.H. Bitter, T. Davidian, M. Ruitenbeek, A.I. Dugulan, K.P. de Jong, J. Am. Chem. Soc. 134 (2012) 16207.
[19] G. Zhou, T. Wu, H. Xie, X. Zheng, Int. J. Hydrog. Energy 38 (2013) 10012.
[20] J.L. Falconer, A.E. Zagli, J. Catal. 62 (1980) 280.
[21] G.D. Weatherbee, C.H. Bartholomew, J. Catal. 77 (1982) 460.
[22] D.E. Peebles, D.W. Goodman, J.M. White, J. Phys. Chem. 87 (1983) 4378.
[23] S. Fujita, H. Terunuma, H. Kobayashi, N. Takezawa, React. Kinet. Catal. Lett. 33 (1987) 179.
[24] C. Schild, A. Wokaun, A. Baiker, J. Mol. Catal. 63 (1990) 243.

[25] R.A.D. Betta, M. Shelef, J. Catal. 48 (1977) 111.
[26] A.H. Karim, A.A. Jalil, S. Triwahyono, S.M. Sidik, N.H.N. Kamarudin, R. Jusoh, N.W.C. Jusoh, B.H. Hameed, J. Colloid Interface Sci. 386 (2012) 307.
[27] X. Yang, D. Chen, S. Liao, H. Song, Y. Li, Z. Fu, Y. Su, J. Catal. 291 (2012) 36.
[28] J. Okal, M. Zawadzki, K. Baranowska, Appl. Catal. A 471 (2014) 98.
[29] R. Moraes, K. Thomas, S. Thomas, S.V. Donk, G. Grasso, J.-P. Gilson, M. Houalla, J. Catal. 299 (2013) 30.
[30] J.H. de Boer, B.G. Linsen, T.J. Osinga, J. Catal. 4 (1965) 643.
[31] Z. Gao, I. Zharov, Chem. Mater. 26 (2014) 2030.
[32] N.W.C. Jusoh, A.A. Jalil, S. Triwahyono, H.D. Setiabudi, N. Sapawe, M.A.H. Satar, A.H. Karim, N.H.N. Kamarudin, R. Jusoh, N.F. Jaafar, N. Salamun, J. Efendi, Appl. Catal. A 468 (2013) 276.
[33] J. Kučera, P. Nachtigall, J. Phys. Chem. B 108 (2004) 16012.
[34] J.A. Wang, O. Novaro, X. Bokhimi, T. López, R. Gómez, J. Navarrete, M.E. Llanos, E. López-Salinas, J. Phys. Chem. B 101 (1997) 7448.
[35] M.J. Climent, A. Corma, S. Iborra, K. Epping, A. Velty, J. Catal. 225 (2004) 316.
[36] J.C. Lavalley, Catal. Today 27 (1996) 377.
[37] C. Drouilly, J.-M. Krafft, F. Averseng, H. Lauron-Pernot, D. Bazer-Bachi, C. Chizallet, V. Lecocq, G. Costentin, Appl. Catal., A 453 (2013) 121.
[38] K.B. Kester, E. Zagli, J.L. Falconer, Appl. Catal. 22 (1986) 311.
[39] P. Riani, G. Garbarino, M.A. Lucchini, F. Canepa, G. Busca, J. Mol. Catal. A: Chem. 383–384 (2014) 10.
[40] S. Mochizuki, M. Satoh, Phys. Status Solidi B 106 (1981) 667.
[41] S. Medsford, J. Chem. Soc. 123 (1923) 1452.
[42] M.A.A. Aziz, N.H.N. Kamarudin, H.D. Setiabudi, H. Hamdan, A.A. Jalil, S. Triwahyono, J. Nat. Gas Chem. 21 (2012) 29.
[43] S. Wilke, D. Hennig, R. Löber, Phys. Rev. B 50 (1994) 2548.
[44] F. Bozso, G. Ertl, M. Grunze, M. Weiss, Appl. Surf. Sci. 1 (1977) 103.
[45] M. Menetrey, A. Markovits, C. Minot, Surf. Sci. 524 (2003) 49.
[46] K. Tanaka, J.M. White, J. Phys. Chem. 86 (1982) 4708.
[47] K. Walter, O.V. Boyevskaya, D. Wolf, M. Baerns, Catal. Lett. 29 (1994) 261.